

Out-of-plane Edelstein effects: Electric-field induced magnetization in p -wave magnets

Motohiko Ezawa¹

¹*Department of Applied Physics, The University of Tokyo, 7-3-1 Hongo, Tokyo 113-8656, Japan*

(Dated: January 6, 2025)

In-plane magnetization is induced by the Edelstein effect in the Rashba spin-orbit interaction system. However, out-of-plane magnetization is more useful for switching a ferromagnetic memory. We study analytically and numerically electric-field induced magnetization in p -wave magnets with the aid of the Rashba interaction based on a simple two-band model. The out-of-plane magnetization is induced when the Néel vector of the p -wave magnet is along the z direction. We also show that no magnetization is induced in the absence of the Rashba interaction. The electric-field induced magnetization will be useful for future switching technology of ferromagnetic memories based on the p -wave magnet.

Introduction: Multiferroic effects are cross correlation effects in electromagnetic responses[1–3]. One is the electric polarization induced by magnetic-field[4–6] and the other is the magnetization induced by electric field[7–10]. Especially, the latter is important for the flip of a magnetic memory under the control of the external electric field. The Edelstein effect[11, 12] is a promising way for it. It is based on the spin-momentum locked Fermi surface induced by the Rashba interaction[13]. In the presence of the Rashba interaction, the spin direction depends on the angle of the momentum as shown in Fig.1(a), where the Fermi surface forms a perfect circle. By applying in-plane electric field, the Fermi distribution is shifted, which induces the imbalance in the spin accumulation. It results in the net in-plane magnetization. However, out-of-plane magnetization is desirable for practical applications to ferromagnetic memories because ferromagnet points to out-of-plane direction. The Edelstein effect is confirmed in various experiments[14–16]. It is also realized in semiconductors[17, 18], Rashba-Dresselhaus systems[19, 20], topological insulators[21, 22], Weyl semimetals[23].

Recently, a p -wave magnet was proposed based on first-principle calculations[24], where the Fermi surface has the p -wave symmetry. A material candidate is CeNiAsO. The system is described by a four-band tight-binding model. Subsequently, the Edelstein effect without the Rashba interaction was proposed in this magnet[25].

In this paper, we investigate the Edelstein effect in a two-dimensional system made of a p -wave magnet with the Rashba interaction, which is described by a simple two-band continuum model. By applying an in-plane electric field, we demonstrate the emergence of the out-of-plane magnetization provided the Néel vector of the p -wave magnet is taken perpendicular to the plane. Namely, it is possible to switch the out-of-plane magnetization by controlling the external in-plane electric field. It would be useful for the switch of a ferromagnetic memory. Our results will open a new way to the magnetic-memory switching device by electric field.

Edelstein effect: The magnetization is induced by the change of the Fermi distribution in the Rashba system, which is called the Edelstein effect. We study such an effect by controlling external electric field \mathbf{E} . We expand the Fermi distribution in powers of \mathbf{E} , $f = f^{(0)} + f^{(1)} + \dots$, where $f^{(0)} = 1/(\exp[(\varepsilon - \mu)/k_B T] + 1)$ is the Fermi distribution func-

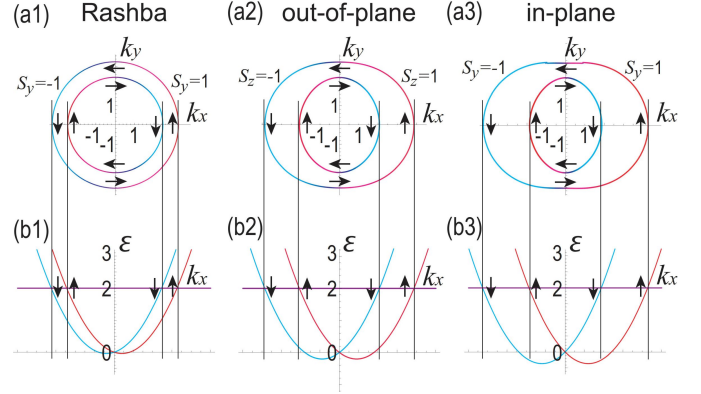


FIG. 1. (a1), (a2) and (a3) Fermi surfaces at $\mu = 2\varepsilon_0$ in the (k_x, k_y) plane. The momentum axis is in units of k_0 . (b1), (b2) and (b3) Energy spectrum along the x axis. The vertical axis is the energy ε in units of ε_0 , while the horizontal axis is k_x in units of k_0 . Purple lines represent $\mu = 2\varepsilon_0$. (a1) and (b1) Rashba model. (a2) and (b2) Out-of-plane p -wave magnet. (a3) and (b3) In-plane p -wave magnet. Red color represents $S_y = 1$, while cyan color represents $S_y = -1$ in (a1), (b1), (a3) and (b3). On the other hand, red color represents $S_z = 1$, while cyan color represents $S_z = -1$ in (a2) and (b2). Arrows represent the spin direction. We have set $m = 4\hbar^2 k_0^2 / \varepsilon_0$, $J = 0.4\varepsilon_0 / k_0$ and $\lambda = 0.2\varepsilon_0 / k_0$.

tion, μ is the chemical potential, ε is the energy, and $f^{(1)}$ is the first-order perturbed Fermi distribution function as a function of \mathbf{E} . By solving the Boltzmann equation, it is explicitly given by

$$f^{(1)} = \frac{e\tau}{\hbar} \mathbf{E} \cdot \nabla_{\mathbf{k}} f^{(0)}, \quad (1)$$

where τ is the relaxation time. We focus on the linear response.

The magnetization is given by the formula[25–36]

$$\mathbf{M} = \frac{e\tau}{\hbar} g\mu_B \int \frac{d^3k}{(2\pi)^3} \mathbf{S}(\mathbf{k}) f^{(1)}, \quad (2)$$

where $\mathbf{S}(\mathbf{k}) \equiv \langle \psi_{\mathbf{k}} | \boldsymbol{\sigma} | \psi_{\mathbf{k}} \rangle$ is the expectation value of the spin operator $\boldsymbol{\sigma}$, g is the g factor, and μ_B is the Bohr magneton. The magnetization formula is rewritten as

$$\mathbf{M} = \frac{e\tau}{\hbar} g\mu_B \int \frac{d^3k}{(2\pi)^3} \mathbf{S}(\mathbf{k}) (\mathbf{E} \cdot \nabla_{\mathbf{k}} \varepsilon) \frac{\partial}{\partial \varepsilon} f^{(0)}. \quad (3)$$

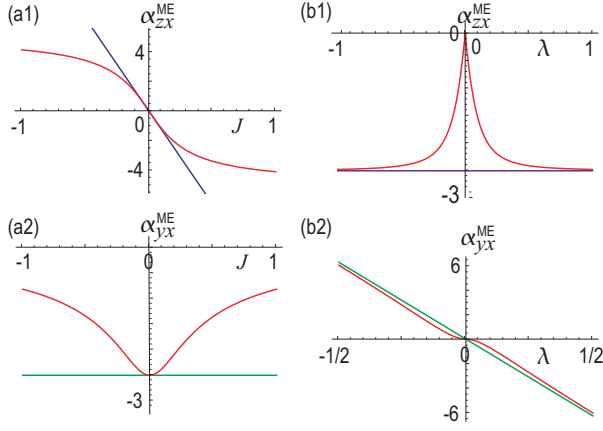


FIG. 2. Out-of-plane Edelstein effect. (a1) α_{zx}^{ME} and (a2) α_{yx}^{ME} as a function of J . We have set $\lambda = 0.2\varepsilon_0/k_0$. (b1) α_{zx}^{ME} and (b2) α_{yx}^{ME} as a function of λ . We have set $J = 0.2\varepsilon_0/k_0$. Red curves represent the numerical results without using the perturbation theory. Blue and green lines represent the analytic results for α_{zx}^{ME} and α_{yx}^{ME} in Eq.(13), respectively. α_{zx}^{ME} , α_{yx}^{ME} and α_{xx}^{ME} are in units of $\frac{g\mu_B k_0}{\hbar W}$, while J and λ are in units of ε_0/k_0 . We have set $\mu = 2\varepsilon_0$ and $m = 4\hbar^2 k_0^2/\varepsilon_0$.

At zero temperature, it is given by

$$\mathbf{M} = e\tau g\mu_B \int \frac{d^3k}{(2\pi)^3} \mathbf{S}(\mathbf{k}) (\mathbf{E} \cdot \mathbf{v}) \delta(\varepsilon_{\mathbf{k}} - \mu), \quad (4)$$

where we have defined the velocity operator $\hbar\mathbf{v} = \nabla_{\mathbf{k}}\varepsilon$.

We apply the electric field along the x axis in the two-dimensional system. When there are two Fermi surfaces $k_{\pm}(\phi)$ around the origin as illustrated in Fig.1, it is rewritten as

$$\mathbf{M} = \frac{e\tau g\mu_B E_x}{(2\pi)^2 W} \sum_{\pm} \int k dk d\phi \mathbf{S}(\mathbf{k}) v_x \frac{\delta(k_{\pm}(\phi) - k)}{\left|\frac{\partial\varepsilon}{\partial k}\right|}, \quad (5)$$

or

$$M_i = e\tau \alpha_{ij}^{\text{ME}} E_j, \quad (6)$$

in terms of the magnetoelectric susceptibility α_{ij}^{ME} given by

$$\alpha_{ix}^{\text{ME}} = \frac{g\mu_B}{(2\pi)^2 W} \sum_{\pm} \int d\phi \frac{k v_x S_i(\mathbf{k})}{\left|\frac{\partial\varepsilon}{\partial k}\right|} \Bigg|_{k=k_{\pm}(\phi)}, \quad (7)$$

where $k_{\pm}(\phi)$ is obtained by solving $\varepsilon(k_{\pm}(\phi)) = \mu$, $v_x = \frac{\partial\varepsilon}{\hbar\partial k_x}$ is the velocity along the x axis, $W^{-1} \equiv \int dk/(2\pi)$ is the width of the sample, and we have introduced the polar coordinate $k_x = k \cos \phi$, $k_y = k \sin \phi$.

Out-of-plane p -wave Edelstein effects: We consider a two-dimensional system made of the p -wave magnet with the Rashba interaction. The simplest model is a two-band model consisting of the free-electron term, the Rashba term[37–45] and the p -wave term[24, 37, 46–49], which is realized as a heterostructure of a magnet on a substrate. The Hamiltonian is given by[37],

$$H(\mathbf{k}) = \frac{\hbar^2(k_x^2 + k_y^2)}{2m} \sigma_0 + \lambda(k_x \sigma_y - k_y \sigma_x) + J k_x \mathbf{n} \cdot \boldsymbol{\sigma}, \quad (8)$$

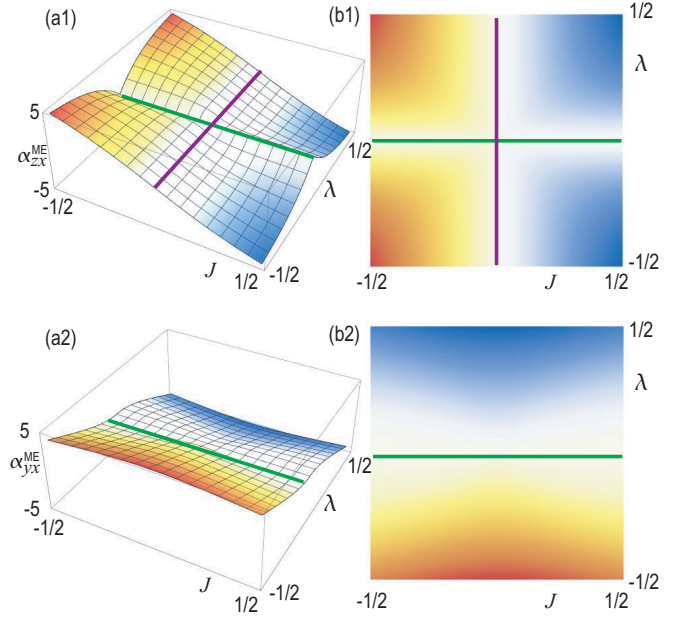


FIG. 3. Out-of-plane Edelstein effect. (a1) Bird's eye's view of α_{zx}^{ME} in the J - λ plane, and (b1) its color plot. (a2) Bird's eye's view of α_{yx}^{ME} in the J - λ plane, and (b2) its color plot. Green line represents the condition $\lambda = 0$ and the purple line represents the condition $J = 0$. See the caption of Fig.2 for the units of various variables. We have set $\mu = 2\varepsilon_0$ and $m = 4\hbar^2 k_0^2/\varepsilon_0$.

where m is the effective mass of free electrons, λ is the magnitude of the Rashba interaction, and \mathbf{n} is the p -wave Néel vector with J its magnitude. The Rashba interaction is introduced by placing a sample on the substrate. We study the case where the Néel vector is along the z direction, $\mathbf{n} = (0, 0, 1)$.

The energy spectrum is given by

$$\varepsilon_{\pm} = \frac{\hbar^2 k^2}{2m} \pm k \sqrt{F(\phi)}, \quad (9)$$

with

$$F(\phi) \equiv \lambda^2 + J^2 \cos^2 \phi. \quad (10)$$

The expectation value of the spin operator $\mathbf{S}(\mathbf{k})$ is determined as

$$S_x^{\pm} = \mp \frac{\lambda \sin \phi}{\sqrt{F(\phi)}}, \quad S_y^{\pm} = \pm \frac{\lambda \cos \phi}{\sqrt{F(\phi)}}, \quad S_z^{\pm} = \pm \frac{J \cos \phi}{\sqrt{F(\phi)}}, \quad (11)$$

which does not depend on k and shown in Fig.1(a3).

The integrand of Eq.(5) is given analytically. By integrating it over ϕ numerically, we obtain the susceptibility α_{ix}^{ME} . We show the components α_{zx}^{ME} and α_{yx}^{ME} in Fig.2, while $\alpha_{xx}^{\text{ME}} = 0$.

We derive an analytic formula for the susceptibility up to the first-order in J and λ . There are two Fermi surfaces $k_{\pm}(\phi)$ as shown in Fig.1(a). The outer Fermi surface $k_-(\phi)$ and the inner Fermi surface $k_+(\phi)$ are given by

$$\hbar k_{\pm}(\phi) = \sqrt{2\mu m} \mp m J \cos \phi, \quad (12)$$

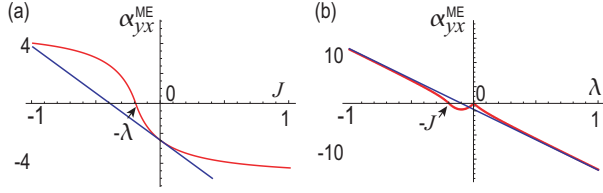


FIG. 4. In-plane Edelstein effect. (a) α_{yx}^{ME} as a function of J . We have set $\lambda = 0.2\varepsilon_0/k_0$. (b) α_{yx}^{ME} as a function of λ . We have set $J = 0.2\varepsilon_0/k_0$. Red curves represent the numerical results without using the perturbation theory. Blue lines represent the analytic results Eq. (18) based on the perturbation theory. See the caption of Fig.2 for the units of various variables. We have set $\mu = 2\varepsilon_0$ and $m = 4\hbar^2 k_0^2/\varepsilon_0$.

which are shown in color in Fig.1(a). The y spin polarization is maximized along the x axis ($\phi = 0, \pi$).

The susceptibility (7) is calculated as

$$\alpha_{xx}^{\text{ME}} = 0, \quad \alpha_{yx}^{\text{ME}} = -\frac{g\mu_B m}{2\pi\hbar^3 W} \lambda, \quad \alpha_{zx}^{\text{ME}} = -\frac{g\mu_B m}{2\pi\hbar^3 W} J \quad (13)$$

for $\mu > 0$ up to the first order in J and λ , which are shown as the blue and green lines in Fig.2, respectively.

We show the numerically obtained susceptibility in the J - λ plane in Fig.3. Eq.(13) agrees well with the numerical result for small J/λ . We find that $\alpha_{zx}^{\text{ME}} = 0$ along the lines $J = 0$ and $\lambda = 0$ as in Fig.3(b1), while $\alpha_{yx}^{\text{ME}} = 0$ along the line $\lambda = 0$. The susceptibility α_{zx}^{ME} is positive for $J < 0$ and negative for $J > 0$, where the sign of α_{zx}^{ME} does not depend on λ . On the other hand, α_{yx}^{ME} is positive for $\lambda < 0$ and negative for $\lambda > 0$, where the sign of α_{yx}^{ME} does not depend on J .

In-plane p -wave magnet: We next study the case where the Néel vector is along the y direction. The energy spectrum is given by

$$\varepsilon_{\pm} = \frac{\hbar^2 k^2}{2m} \pm k\sqrt{G(\phi)}, \quad (14)$$

with

$$G(\phi) \equiv \lambda^2 \sin^2 \phi + (J + \lambda)^2 \cos^2 \phi. \quad (15)$$

The Fermi surface is shown in Fig.1(a3). There are two Fermi surfaces $k_{\pm}(\phi)$. The outer Fermi surface $k_{-}(\phi)$ and the inner Fermi surface $k_{+}(\phi)$ are analytically given by

$$\hbar k_{\pm}(\phi) = \sqrt{2\mu m} \mp m\lambda + J \left(m \mp \frac{m\sqrt{m\lambda}}{\sqrt{2\mu}} \right) \cos^2 \phi \quad (16)$$

up to the first order in J and λ . The spin direction is

$$S_{\pm}^y = \pm \frac{(J + \lambda)x}{\sqrt{G(\phi)}}. \quad (17)$$

The susceptibility (7) is calculated as

$$\alpha_{yx}^{\text{ME}} = -\frac{mg\mu_B}{4\pi\hbar^3 W} (J + 2\lambda), \quad \alpha_{xx}^{\text{ME}} = \alpha_{zx}^{\text{ME}} = 0 \quad (18)$$

for $\mu > 0$ up to the first order in J and λ , which is shown as the blue lines in Fig.4.

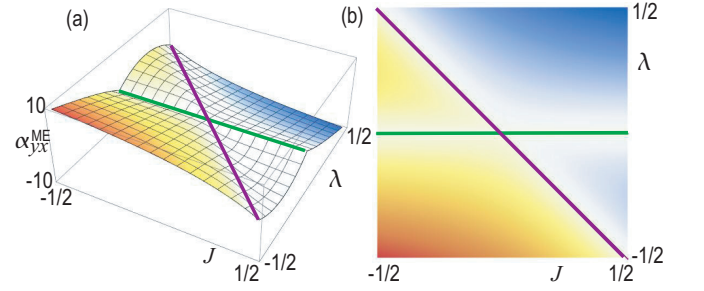


FIG. 5. In-plane Edelstein effect. Bird's eye's view of α_{yx}^{ME} in the J - λ plane, and (b) its color plot. Green line represents the condition $\lambda = 0$ and the purple line represents the condition $\lambda + J = 0$. See the caption of Fig.2 for the units of various variables. We have set $\mu = 2\varepsilon_0$ and $m = 4\hbar^2 k_0^2/\varepsilon_0$.

We show the numerically obtained susceptibility in Fig.4. Eq.(18) agrees well with the numerical result for small J/λ . The susceptibility is zero $\alpha_{ix}^{\text{ME}} = 0$ for $\lambda = 0$ or $J + \lambda = 0$ as shown in Fig.4(a) and (b), where the Hamiltonian (8) is diagonal. The susceptibility α_{yx}^{ME} is positive for $J + \lambda < 0$ and negative for $J + \lambda > 0$ as shown in in Fig.5(a) and (b). It is because the spin direction along the x axis matters for the electric-field induced magnetization. On the other hand, the sign of the susceptibility α_{yx}^{ME} does not change at $\lambda = 0$ because $f^{(1)}(0, k_y) = 0$.

Discussion: We investigated the electric-field induced magnetization in a simple two-band p -wave magnet model, where the Rashba interaction is essential. On the other hand, the electric-field induced magnetization was shown to occur without the Rashba interaction in the p -wave magnet system described by the four-band model[24, 25]

$$H = 2t \left(\tau_x \cos \frac{k_x}{2} + \cos k_y \right) + 2t_J \left(\sigma_x \tau_y \sin \frac{k_x}{2} + \sigma_y \tau_z \cos k_y \right), \quad (19)$$

where σ and τ correspond to the spin and site degrees of freedom.

The above four-band model is derived for a specific material candidate CeNiAsO[24], which is a metal. The dependence of the pseudospin τ enters in a specific way, and hence, this four-band Hamiltonian is applicable to a specific case. On the other hand, the two-band Hamiltonian (8) is quite universal. There are two possibilities to realize the model. One is the metallic p -wave magnet without the pseudospin degrees of freedom on a substrate producing the Rashba interaction. The other is the insulating p -wave magnet, where free electrons exist away from the p -wave magnet, while the interface produces the Rashba interaction. Our results will open a new way to multiferroics based on the p -wave magnet.

This work is supported by CREST, JST (Grants No. JPMJCR20T2) and Grants-in-Aid for Scientific Research from MEXT KAKENHI (Grant No. 23H00171).

- [1] M. Fiebig, Revival of the magnetoelectric effect, *J. Phys. D: Appl. Phys.* 38 R123 (2005).
- [2] W. Eerenstein, N. D. Mathur and J. F. Scott, Multiferroic and magnetoelectric materials, *Nature* 442, 759 (2006).
- [3] R. Ramesh and Nicola A. Spaldin, Multiferroics: progress and prospects in thin films *Nature Materials* 6, 21 (2007).
- [4] T. Kimura, T. Goto, H. Shintani, K. Ishizaka, T. Arima and Y. Tokura, Magnetic control of ferroelectric polarization, *Nature* 426, 55 (2003).
- [5] N. Hur, S. Park, P. A. Sharma, J. S. Ahn, S. Guha and S-W. Cheong, Electric polarization reversal and memory in a multiferroic material induced by magnetic fields, *Nature* 429, 392 (2004).
- [6] Ce-Wen Nan, Gang Liu, and Yuanhua Lin and Haydn Chen, Magnetic-Field-Induced Electric Polarization in Multiferroic Nanostructures, *Phys. Rev. Lett.* 94, 197203 (2005).
- [7] H. Ohno, D. Chiba, F. Matsukura, T. Omiya, E. Abe, T. Dietl, Y. Ohno and K. Ohtani, Electric-field control of ferromagnetism, *Nature* 408, 944 (2000).
- [8] Ying-Hao Chu, Lane W. Martin, Mikel B. Holcomb, Martin Gajek, Shu-Jen Han, Qing He, Nina Balke, Chan-Ho Yang, Donkoun Lee, Wei Hu, Qian Zhan, Pei-Ling Yang, Arantxa Fraile-Rodriguez, Andreas Scholl, Shan X. Wang and R. Ramesh, Electric-field control of local ferromagnetism using a magnetoelectric multiferroic, *Nature Materials* 7, 478 (2008).
- [9] J. T. Heron, M. Trassin, K. Ashraf, M. Gajek, Q. He, S. Y. Yang, D. E. Nikonov, Y-H. Chu, S. Salahuddin and R. Ramesh, Electric-Field-Induced Magnetization Reversal in a Ferromagnet-Multiferroic Heterostructure, *Phys. Rev. Lett.* 107, 217202 (2011).
- [10] Fumihiro Matsukura, Yoshinori Tokura, Hideo Ohno, Control of magnetism by electric fields, *Nature Nanotechnology* 10, 209 (2015).
- [11] V.M. Edelstein, Spin polarization of conduction electrons induced by electric current in two-dimensional asymmetric electron systems, *Solid State Communications* 73 (3): 233 (1990).
- [12] P. Gambardella and I. M. Miron, Current-induced spin-orbit torques, *Philos. Trans. R. Soc. A Math. Phys. Eng. Sci.* 369, 3175 (2011).
- [13] A. Manchon, H. C. Koo, J. Nitta, S. M. Frolov, and R. A. Duine, New perspectives for rashba spin-orbit coupling, *Nat. Mater.* 14, 871 (2015).
- [14] J. C. Rojas-Sanchez, L. Vila, G. Desfonds, S. Gambarelli, J.P. Attane, J. M. De Teresa, C. Magen, A. Fert, Spin-to-charge conversion using Rashba coupling at the interface between non-magnetic materials, *Nature Communications* 4, 2944 (2013).
- [15] H. J. Zhang, S. Yamamoto, B. Gu, H. Li, M. Maekawa, Y. Fukaya, and A. Kawasuso, Charge-to-Spin Conversion and Spin Diffusion in Bi/Ag Bilayers Observed by Spin-Polarized Positron Beam, *Phys. Rev. Lett.* 114, 166602 (2015).
- [16] Ye Du, Hiromu Gamou, Saburo Takahashi, Shutaro Karube, Makoto Kohda, and Junsaku Nitta, Disentanglement of Spin-Orbit Torques in Pt/Co Bilayers with the Presence of Spin Hall Effect and Rashba-Edelstein Effect, *Phys. Rev. Applied* 13, 054014 (2020).
- [17] Y. Kato, R. C. Myers, A. C. Gossard, and D. D. Awschalom, Coherent spin manipulation without magnetic fields in strained semiconductors, *Nature* 427, 50 (2004).
- [18] R. Peters and Y. Yanase, Strong enhancement of the Edelstein effect in f -electron systems, *Phys. Rev. B* 97, 115128 (2018).
- [19] V. V. Bryksin and P. Kleinert, Theory of electric-field-induced spin accumulation and spin current in the two-dimensional Rashba model, *Phys. Rev. B - Condens. Matter Mater. Phys.* 73, 1 (2006).
- [20] S. Leiva-Montecinos, J. Henk, I. Mertig, and A. Johansson, Spin and orbital Edelstein effect in a bilayer system with Rashba interaction, *Phys. Rev. Res.* 5, 1 (2023).
- [21] A. R. Mellnik, J. S. Lee, A. Richardella, J. L. Grab, P. J. Mintun, M. H. Fischer, A. Vaezi, A. Manchon, E.-A. Kim, N. Samarth & D. C. Ralph Spin-transfer torque generated by a topological insulator, *Nature* volume 511, 449 (2014).
- [22] J.-C. Rojas-Sanchez, S. Oyarzun, Y. Fu, A. Marty, C. Vergnaud, S. Gambarelli, L. Vila, M. Jamet, Y. Ohtsubo, A. Taleb-Ibrahimi, P. Le Fevre, F. Bertran, N. Reyren, J.-M. George, A. Fert, Spin-pumping into surface states of topological insulator α -Sn, spin to charge conversion at room temperature, *Phys. Rev. Lett.* 116, 096602 (2016).
- [23] A. Johansson, J. Henk, and I. Mertig, Edelstein effect in Weyl semimetals, *Phys. Rev. B* 97, 1 (2018).
- [24] Anna Birk Hellenes, Tomas Jungwirth, Jairo Sinova, Libor Šmejkal, Unconventional p-wave magnets, arXiv:2309.01607.
- [25] Atasi Chakraborty, Anna Birk Hellenes, Rodrigo Jaeschke-Ubiergo, Tomas Jungwirth, Libor Šmejkal, Jairo Sinova, Highly Efficient Non-relativistic Edelstein effect in p-wave magnets, arXiv:2411.16378.
- [26] I. Garate, K. Gilmore, M. D. Stiles, and A. H. MacDonald, Nonadiabatic spin-transfer torque in real materials, *Phys. Rev. B* 79, 104416 (2009).
- [27] Ion Garate, A.H. MacDonald, Influence of a Transport Current on Magnetic Anisotropy in Gyrotropic Ferromagnets, *Phys. Rev. B* 80, 134403 (2009).
- [28] J. Zelezny, H. Gao, K. Vyborny, J. Zemen, J. Masek, A. Manchon, J. Wunderlich, J. Sinova, and T. Jungwirth, Relativistic Neel-order fields induced by electrical current in antiferromagnets, *Phys. Rev. Lett.* 113, 1 (2014).
- [29] Hang Li, H. Gao, Liviu P. Zarbo, K. Vyborny, Xuhui Wang, Ion Garate, Fatih Dogan, A. Cejchan, Jairo Sinova, T. Jungwirth, Aurelien Manchon, Intradband and interband spin-orbit torques in noncentrosymmetric ferromagnets, *Phys. Rev. B* 91, 134402 (2015).
- [30] A. Manchon, J. Zelezny, I. M. Miron, T. Jungwirth, J. Sinova, A. Thiaville, K. Garello, and P. Gambardella, Current-induced spin-orbit torques in ferromagnetic and antiferromagnetic systems, *Reviews of Modern Physics* 91, 035004 (2019).
- [31] Karma Tenzin, Arunesh Roy, Frank T. Cerasoli, Anooja Jayaraj, Marco Buongiorno Nardelli, Jagoda Sławińska, Collinear Rashba-Edelstein effect in non-magnetic chiral materials, *Phys. Rev. B* 108, 245203 (2023).
- [32] R. Gonzalez-Hernandez, P. Ritzinger, K. Vyborny, J. Zelezny, and A. Manchon, Non-relativistic torque and edelstein effect in non-collinear magnets, *Nature Communications* 15, 1 (2024).
- [33] Y. Chen, Z. Z. Du, H.-Z. Lu, and X. C. Xie, Intrinsic spin-orbit torque mechanism for deterministic all-electric switching of noncollinear antiferromagnets, *Phys. Rev. B* 109, L121115 (2024).
- [34] Mattia Trama, Irene Gaiardoni, Claudio Guarcello, Jorge I. Facio, Alfonso Maiellaro, Francesco Romeo, Roberta Citro, Jeroen van den Brink, Non-linear anomalous Edelstein response at altermagnetic interfaces, arXiv:2410.18036.
- [35] Mengli Hu, Oleg Janson, Claudia Felser, Paul McClarty, Jeroen van den Brink, Maia G. Vergniory, Spin Hall and Edelstein Effects in Novel Chiral Noncollinear Altermagnets,

- arXiv:2410.17993.
- [36] Nayra A. Alvarez Pari, Rodrigo Jaeschke-Ubiergo, Atasi Chakraborty, Libor Smejkal and Jairo Sinova, Non-relativistic linear Edelstein effect in non-collinear EuIn_2As_2 , arXiv:2412.10984.
- [37] M. Ezawa, Purely electrical detection of the Neel vector of p-wave magnets based on linear and nonlinear conductivities, arXiv:2410.21854.
- [38] L. Smejkal, A. H. MacDonald, J. Sinova, S. Nakatsuji and T. Jungwirth, Anomalous Hall antiferromagnets, *Nat. Rev. Mater.* 7, 482 (2022).
- [39] Libor Šmejkal, Jairo Sinova, and Tomas Jungwirth, Emerging Research Landscape of Altermagnetism, *Phys. Rev. X* 12, 040501 (2022).
- [40] Di Zhu, Zheng-Yang Zhuang, Zhigang Wu, and Zhongbo Yan, Topological superconductivity in two-dimensional altermagnetic metals, *Phys. Rev. B* 108, 184505 (2023).
- [41] Chi Sun, Jacob Linder, Spin pumping from a ferromagnetic insulator into an altermagnet, *Phys. Rev. B* 108, L140408 (2023).
- [42] G. S. Diniz and E. Vernek, Suppressed Kondo screening in two-dimensional altermagnets, *Phys. Rev. B* 109, 155127 (2024).
- [43] Peng Rao, Alexander Mook, Johannes Knolle, Tunable band topology and optical conductivity in altermagnets, *Phys. Rev. B* 110, 024425 (2024).
- [44] Morten Amundsen, Arne Brataas, Jacob Linder, RKKY interaction in Rashba altermagnets, *Phys. Rev. B* 110, 054427 (2024).
- [45] M. Ezawa, Detecting the Neel vector of altermagnets in heterostructures with a topological insulator and a crystalline valley-edge insulator, *Phys. Rev. B* 109 (24), 245306 (2024).
- [46] Kazuki Maeda, Bo Lu, Keiji Yada, Yukio Tanaka, Theory of tunneling spectroscopy in p-wave altermagnet-superconductor hybrid structures, *J. Phys. Soc. Jpn.* 93, 114703 (2024).
- [47] M. Ezawa, Topological insulators based on *p*-wave altermagnets; Electrical control and detection of the altermagnetic domain wall, *Phys. Rev. B* 110, 165429 (2024).
- [48] Bjonulf Brekke, Pavlo Sukhachov, Hans Glokner Giil, Arne Brataas, Jacob Linder, Minimal models and transport properties of unconventional p-wave magnets, *Phys. Rev. Lett.* 133, 236703 (2024).
- [49] M. Ezawa, Third-order and fifth-order nonlinear spin-current generation in g-wave and i-wave altermagnets and perfect spin-current diode based on f-wave magnets, arXiv:2411.16036.